^{13}C n.m.r. isotopomer and computer-simulation studies of the non-oxidative pentose phosphate pathway of human erythrocytes

Hilary A. BERTHON, William A. BUBB and Philip W. KUCHEL*
Department of Biochemistry, University of Sydney, Sydney, NSW 2006, Australia

^{13}C double-quantum filtered correlation spectroscopy (DQF-COSY) provides a novel method for the detection of reactions involving carbon-bond scissions. We report the use of this technique to investigate isotopic exchange reactions of the non-oxidative pentose phosphate pathway in human erythrocytes. These exchange reactions resulted in the formation of a range of isotopic isomers (isotopomers) of glucose 6-phosphate after incubation of a mixture of universally ^{13}C-labelled and unlabelled glucose 6-phosphate with fructose 1,6-bisphosphate and haemolysates. These isotopomers were detected in the coupling patterns of cross-peaks within the DQF-COSY spectrum of the deproteinized sample. A computer model which fully describes the reactions of the non-oxidative pentose phosphate pathway in human erythrocytes has previously been constructed and tested with ^{31}P n.m.r. time-course data in our laboratory. This model was refined using ^{13}C n.m.r. time-course data and extended to include the range of isotopomers which may be formed experimentally by the reactions of the non-oxidative pentose phosphate pathway. The isotopomer ratios obtained experimentally from the DQF-COSY spectrum were consistent with simulations generated by this model.

INTRODUCTION

Owing to the low natural abundance of the ^{13}C nucleus, the study of biological systems with ^{13}C n.m.r. has largely depended upon the use of isotopically substituted substrates (Scott and Baxter, 1981). Although in many respects metabolic n.m.r. experiments with ^{13}C-labelled substrates resemble the studies which may be performed with ^{14}C-labelled compounds (Cohen et al., 1981), ^{13}C n.m.r. has the additional capability of yielding information on label correlations via ^{13}C–^{13}C homonuclear coupling patterns. Observation of the labelling patterns can yield information about the incorporation of complex structural units: the technique of diluting a multiply substituted substrate with substrate at natural abundance introduces the means of detecting carbon-bond scissions and thus observing carbon-group-transfer reactions. We describe here the novel use of an n.m.r. technique, ^{13}C double-quantum filtered correlation spectroscopy (DQF-COSY), to detect the distribution of isotopic forms of glucose 6-phosphate (Glc6*P*) arising from the incubation of [U-^{13}C]Glc6*P*, Glc6*P* and fructose 1,6-bisphosphate [Fru(1,6)P_2] with a haemolysate. This approach was pioneered by Jones and Sanders (1989) in their study of the biosynthetic origins of the *Klebsiella* K3 serotype polysaccharide. In the present study we have observed the range of coupling patterns within cross-peaks of a ^{13}C DQF-COSY spectrum, to evaluate the range of isotopomers formed by the non-oxidative pentose phosphate pathway enzyme system in human erythrocytes.

In a COSY experiment, a cross-peak derived from the coupling of two ^{13}C nuclei denoted by A and M, with nuclear coupling constant, J_{AM}, appears as an antiphase doublet. If M is further coupled to a nucleus X, J_{MX}, the passive coupling, is evident in the AM cross-peak (observed at the chemical shift of M in the frequency domain, f_2) and is characterized by its in-phase appearance. The shorthand notation of Jones and Sanders (1989) has been adopted in the ensuing discussion of this experiment: e.g. the cross-peak observed between carbon atoms 4 and 5 of Glc6*P*, at the chemical shift of carbon 4 in f_2 is denoted by C_{45}^{4}, with the corresponding cross-peak at the chemical shift of carbon 5 being denoted by C_{45}^{5}. Overall, the cross-peaks are a combination of superimposed coupling patterns arising from the responses of the various isotopomers present in the sample.

Mathematical models of metabolism, in conjunction with isotopomer analysis, have assisted in the interpretation of n.m.r.-derived data, enabling predictions about the nature of pathway interactions and metabolite preferences to be drawn (e.g., London, 1988; Malloy et al., 1990). We report the results derived from a computer model which incorporates the reactions of isotopically substituted metabolites in the non-oxidative pentose phosphate pathway and which was used to simulate the formation of isotopomers of Glc6*P* which would arise upon incubation of Glc6*P*, [U-^{13}C]Glc6*P* and Fru(1,6)P_2 with a haemolysate. This model was initially tested with data obtained from a ^{13}C n.m.r. time course acquired following the addition of a haemolysate to Glc6*P*, [1-^{13}C]Glc6*P* and Fru(1,6)P_2. The relative concentrations of the isotopic forms detected in the ^{13}C-COSY experiment were compared with the predicted relative concentrations based on computer simulations of the model.

Isotopic-exchange effects have been noted to occur in reactions catalysed by transaldolase (TA) (Ljungdahl et al., 1961), transketolase (TK) (Clark et al., 1971) and aldolase (Bartlett et al., 1989). Along with reversal of the pathway followed by reformation of hexose 6-phosphate, these exchange reactions have

Abbreviations used: DHAP, dihydroxyacetone phosphate; Ery4*P*, erythrose 4-phosphate; *f*, furanose; f.i.d., free induction decay; Fru(1,6)P_2, fructose 1,6-bisphosphate; Fru6*P*, fructose 6-phosphate; G3*P*, glyceraldehyde 3-phosphate; Gal1*P*, galactose 1-phosphate; glm, glycolaldehyde moiety transferred by transketolase; Glc1*P*, glucose 1-phosphate; Glc(1,6)P_2, glucose 1,6-bisphosphate; Glc6*P*, glucose 6-phosphate; grn, dihydroxyacetone moiety transferred by transaldolase; Man6*P*, mannose 6-phosphate; *p*, pyranose; Rib5*P*, ribose 5-phosphate; Ru5*P*, ribulose 5-phosphate; Sed(1,7)P_2, sedoheptulose 1,7-bisphosphate; Sed7*P*, sedoheptulose 7-phosphate; TA, transaldolase (EC 2.2.1.2); TK, transketolase (EC 2.2.1.1); UDP-Gal, UDP-5′-galactose; UDP-Glc, UDP-5′-glucose; Xu5*P*, xylulose 5-phosphate (all sugar phosphates mentioned in this paper are of the D configuration); DQF-COSY, double-quantum filtered correlation spectroscopy; f.i.d., free induction decay.

* To whom correspondence should be addressed.

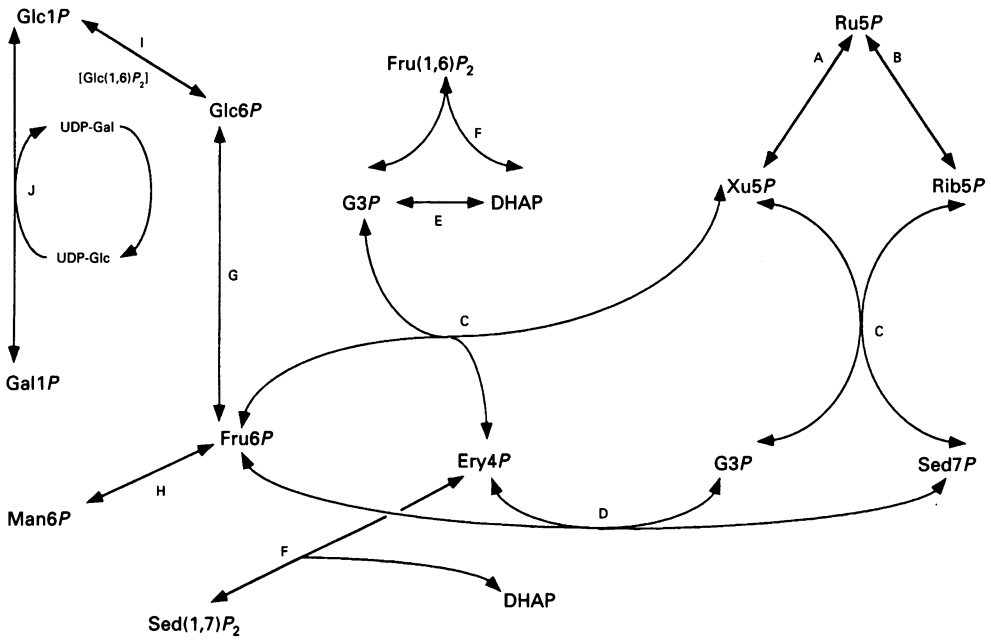

Scheme 1 The reactions of the non-oxidative pentose phosphate pathway used in the computer simulations

The enzymes are: A, ribulose-5-phosphate epimerase; B, ribose-5-phosphate isomerase; C, TK; D, TA; E, triosephosphate isomerase; F, aldolase; G, glucosephosphate isomerase; H, phosphomannose isomerase; I, phosphoglucomutase; J, galactose-1-phosphate uridyltransferase; see also the abbreviations footnote. The mechanisms by which these enzymes are assumed to operate and the definitions of the unitary rate constants and equation numbers are the same as those of McIntyre et al. (1989). The unitary rate constants used in the computer model were (s^{-1} and $M^{-1} \cdot s^{-1}$ for first- and second-order rate constants respectively): A, $k_1 = 3.91 \times 10^6$; $k_2 = 4.38 \times 10^2$; $k_3 = 3.05 \times 10^2$; $k_4 = 1.49 \times 10^6$; B, $k_1 = 7.27 \times 10^4$; $k_2 = 3.138 \times 10^1$; $k_3 = 3.33 \times 10^1$; $k_4 = 8.29 \times 10^4$; C, (eqn. 1): $k_1 = 2.16 \times 10^5$; $k_2 = 5.5 \times 10^1$; $k_3 = 7.7 \times 10^1$; $k_4 = 9.0 \times 10^6$; $k_5 = 3.95 \times 10^5$; $k_6 = 2.53 \times 10^2$; $k_7 = 7.7 \times 10^1$; $k_8 = 1.95 \times 10^3$; (eqn. 2): k_1–k_4 are the same as for eqn. (1); $k_5 = 8.96 \times 10^7$; $k_6 = 2.53 \times 10^2$; $k_7 = 7.7 \times 10^1$; $k_8 = 3.08 \times 10^4$; D, $k_1 = 6.6 \times 10^5$; $k_2 = 4.53 \times 10^1$; $k_3 = 1.63 \times 10^1$; $k_4 = 5.0 \times 10^6$; $k_5 = 4.58 \times 10^6$; $k_6 = 6.0 \times 10^1$; $k_7 = 1.7 \times 10^1$; $k_8 = 1.66 \times 10^5$; E, $k_1 = 3.7 \times 10^7$; $k_2 = 1.32 \times 10^3$; $k_3 = 1.46 \times 10^4$; $k_4 = 1.9 \times 10^7$; F (eqn. 6): $k_1 = 1.07 \times 10^7$; $k_2 = 2.33 \times 10^2$; $k_3 = 1.9 \times 10^3$; $k_4 = 2.8 \times 10^7$; $k_5 = 6.41 \times 10^6$; $k_6 = 7.0 \times 10^1$; (eqn. 4): $k_1 = 8.47 \times 10^6$; $k_2 = 1.51 \times 10^2$; $k_3 = 1.17 \times 10^2$; $k_4 = 4.05 \times 10^6$; $k_5 = 6.41 \times 10^6$; $k_6 = 7.0 \times 10^1$; G, $k_1 = 3.98 \times 10^7$; $k_2 = 1.29 \times 10^3$; $k_3 = 1.55 \times 10^3$; $k_4 = 1.56 \times 10^7$; H, $k_1 = 1.19 \times 10^6$; $k_2 = 8.0 \times 10^2$; $k_3 = 8.0 \times 10^2$; $k_4 = 1.23 \times 10^6$; I, $k_1 = 8.09 \times 10^1$; $k_2 = 4.2 \times 10^6$; $k_3 = 7.2 \times 10^5$; $k_4 = 2.426 \times 10^2$; $k_5 = 1.0 \times 10^1$; $k_6 = 1.3 \times 10^7$; J, $k_1 = 7.58 \times 10^5$; $k_2 = 1.0 \times 10^2$; $k_3 = 1.5 \times 10^2$; $k_4 = 8.75 \times 10^5$; $k_5 = 3.96 \times 10^5$; $k_6 = 1.1 \times 10^2$; $k_7 = 1.13 \times 10^2$; $k_8 = 8.73 \times 10^5$. The enzyme concentrations were ($mol \cdot l^{-1}$): A, 2.96×10^{-6}; B, 6.9×10^{-5}; C, 1.7×10^{-7}; D, 9.1×10^{-7}, E, 7.96×10^{-7}; F, 3.4×10^{-7}; G, 1.40×10^{-7}; H, 1.7×10^{-10}; I, 1.0×10^{-8}; J, 3.36×10^{-8}.

been used to explain labelling patterns which are not in accordance with those predicted assuming irreversibility of the reactions of the non-oxidative pentose phosphate pathway by both the classical (e.g. Ljungdahl et al., 1961; Landau and Bartsch, 1966; Landau and Wood, 1983; Scofield et al., 1985) and the more recently proposed L-type mechanism (e.g. Williams et al., 1971, 1978, 1986; Longenecker and Williams, 1980a,b; Williams, 1980; Williams and Blackmore, 1983; Arora et al., 1987; Butler et al., 1990). The exchange reactions are a special case of the label scrambling which can occur due to the bidirectional nature of the enzymic reactions of the non-oxidative pentose phosphate pathway, and arise as a consequence of the reversibility of the group translocation enzymic reactions. For example, TA catalyses the transfer of a three-carbon unit from Fru6*P* to glyceraldehyde 3-phosphate (G3*P*), resulting in the formation of new Fru6*P* and G3*P* molecules which may have different labelling patterns, namely:

$$[1,2,3,4,5,6\text{-}^{13}C]\text{Fru6}P + \text{G3}P \rightleftharpoons [1,2,3\text{-}^{13}C]\text{G3}P + [1,2,3\text{-}^{13}C]\text{Fru6}P$$

EXPERIMENTAL

Preparation of haemolysates

Freshly drawn blood was obtained from the antecubital vein of a single donor (H.A.B.) by venipuncture and added to heparin (15 units/ml of whole blood; Weddel Pharmaceuticals, Thornleigh, NSW, Australia). Following centrifugation (3000 *g*, 5 min, 4 °C), the supernatant plasma was withdrawn and most of the leucocytes were removed by aspiration. The plasma was then replaced and the suspension of erythrocytes was further diluted by the addition of approx. 3 vol. of cold iso-osmotic NaCl before filtration through a Sepacell R-500N Leucocyte Removal Filter (Asahi Medical Co. Ltd., Tokyo, Japan). The resultant cell suspension was centrifuged again and the supernatant removed by aspiration. The cells were re-suspended in NaCl and the washing procedure repeated twice. The erythrocyte suspension was gently gassed with CO for approx. 15 min before the penultimate centrifugation step; the final wash was with a 0.154 M NaCl solution containing 20% (v/v) ^2H_2O.

Haemolysates were prepared by sonication (3 × 5 s; 40 W output; model B-12 sonifier; Branson, Danbury, CT, U.S.A.) of erythrocyte suspensions (haematocrit 0.92) and were stored at −20 °C. Haemolysates were incubated at 37 °C for 40–45 min before their addition to metabolic substrates. This procedure effects the removal of NAD(P)(H) through the action of $NAD(P)^+$ glycohydrolase (Kuchel and Chapman, 1985), preventing substrate recycling through the oxidative part of the pentose phosphate pathway or removal through glycolysis.

Preparation of [U-^{13}C]Glc6*P* and [1-^{13}C]Glc6*P*

[U-^{13}C]Glc6*P* was enzymically prepared from [U-^{13}C]Glc (Cambridge Isotope Laboratories, Woburn, MA, U.S.A.) by

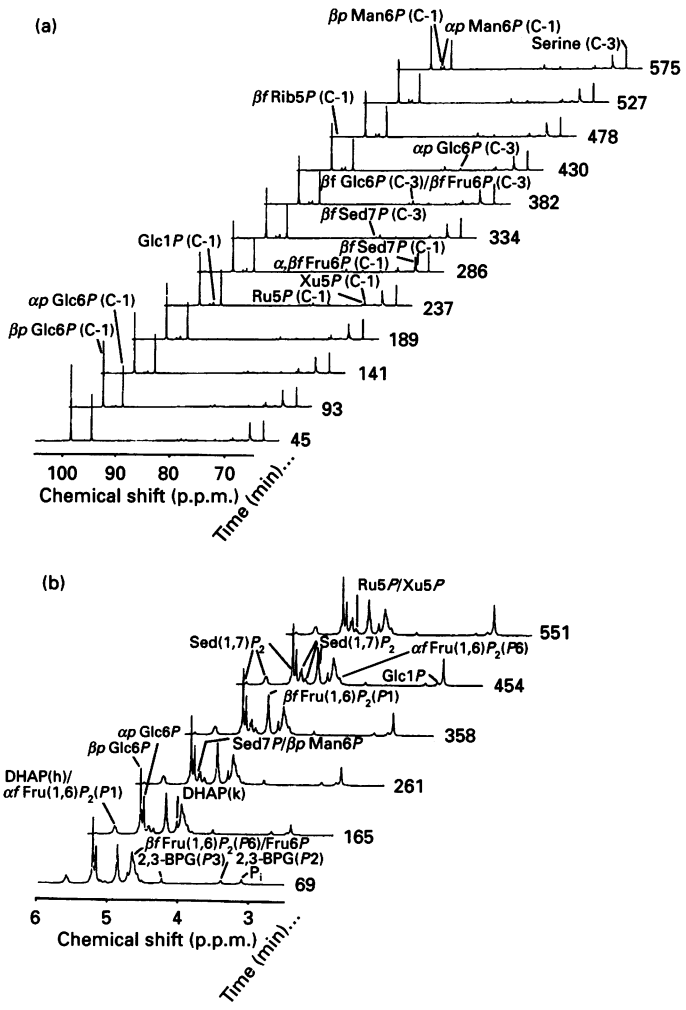

Figure 1 Time courses of ^{13}C-(a) and ^{31}P-(b) n.m.r. spectra acquired after the addition of haemolysates to a sample containing [1-^{13}C]Glc6*P*, Glc6*P* and Fru(1,6)P_2

For sample composition, see the Experimental section. Acquisition parameters: (**a**) spectrometer frequency, 150.919 MHz; number of transients per spectrum, 160; acquisition time, 0.6 s; pulse angle, $\pi/2$; recycle time, 10 s; spectral width, 31 240 Hz; spectra were processed into 64 k data points with an exponential line-broadening factor of 3 Hz; (**b**) spectrometer frequency, 242.943 MHz; number of transients per spectrum, 64; acquisition time, 0.8 s; pulse angle, $\pi/2$; recycle time, 20 s ($5 \times T_1$; Berthon et al., 1992); spectral width, 7353 Hz; spectra were processed into 16 k data points; broadband proton decoupling (WALTZ-16) was applied continuously for both ^{13}C- and ^{31}P-n.m.r. time courses; sample temperature, 37 °C. The times given represent the calculated midpoint time of each spectral accumulation. Abbreviation: 2,3-BPG, 2,3-bisphosphoglycerate; h, hydrate form; k, ketone form; see also the abbreviations footnote.

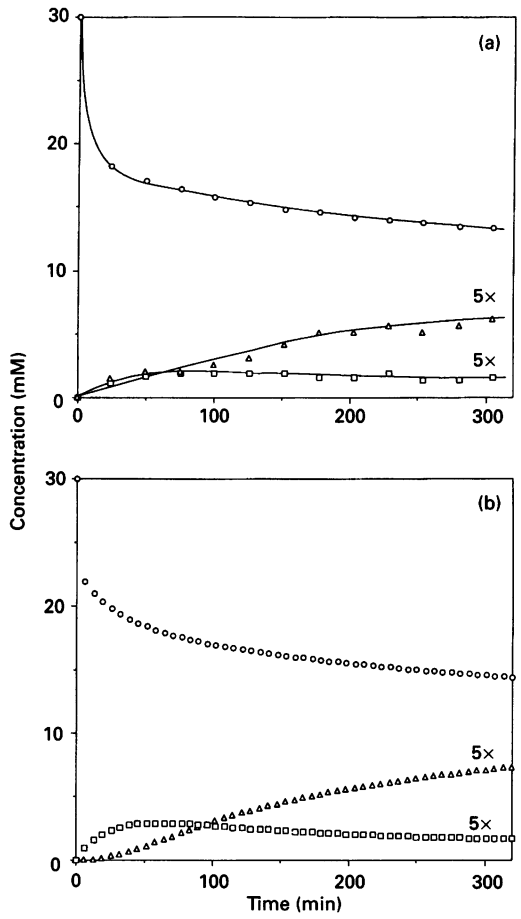

Figure 2 Experimental (a) and simulated (b) metabolite concentration profiles following the incubation of [1-^{13}C]Glc6*P*, Glc6*P* and Fru(1,6)P_2 with haemolysates

For sample composition and n.m.r. acquisition parameters, see the Experimental section and Figure 1. The symbols denote the following: ○, Glc6*P* labelled at C-1; △, Glc6*P* labelled at C-3; □, Ru5*P* labelled at C-1. The time scale for the experimental data has been adjusted for a 100% haematocrit-equivalent. Concentrations were obtained from ^{13}C-n.m.r. time-course spectra by integration of the following resonances: Glc6*P* (C-1), βGlc6*P* C-1 plus αGlc6*P* C-1; Glc6*P* (C-3), αGlc6*P* C-3; and Ru5*P* (C-1), Ru5*P* C-1. Simulations were carried out with initial conditions identical with those present experimentally.

incubation with ATP and hexokinase (EC 2.7.1.1). The phosphorylated product was isolated by anion exchange (AG 1-X8 resin; 100–200 mesh, formate form; Bio-Rad, Richmond, CA, U.S.A.) by applying 1 M ammonium formate/4 M formic acid in a stepwise increasing concentration (Bartlett, 1968). Fractions containing Glc6*P* were identified with the anthrone reagent (Graham and Smydzuk, 1965) and were subsequently pooled and passed through a cation-exchange column (Dowex 50W, H^+ form, Sigma). Continuous extraction with diethyl ether (Paoletti et al., 1979) was used to remove the formic acid eluant. [1-^{13}C]Glc6*P* was prepared from [1-^{13}C]Glc (Cambridge Isotope Laboratories, Woburn, MA, U.S.A.) in an analogous manner. Both [U-^{13}C]Glc6*P* and [1-^{13}C]Glc6*P* were characterized by their ^{1}H- and ^{13}C-n.m.r. spectra.

N.m.r. time-course sample

The time-course sample contained [1-^{13}C]Glc6*P* (30 mM); Fru(1,6)P_2 (30 mM); Glc6*P* (20 mM); [3-^{13}C]serine used as an intensity reference (2.7 mM); haemolysate (900 μl; final haematocrit-equivalent 0.47); triethyl phosphate, methyl phosphonate and triethanolamine buffer [triethanolamine, 50 mM; KCl, 90 mM; NaCl, 10 mM; $MgCl_2$ 2 mM; DL-dithiothreitol, 1 mM; EDTA, 0.5 mM; 10% (v/v) ^2H_2O], pH 7.28.

^{13}C-COSY sample

[U-^{13}C]Glc6*P* (57 μmol), Glc6*P* (38 μmol) and Fru(1,6)P_2 (57 μmol) were dissolved in triethanolamine buffer (1 ml; same composition as given above) with [3-^{13}C]serine and haemolysate (1 ml). The sample (pH 7.4) was incubated for 10 h and then deproteinized by ultrafiltration at 4 °C through a YM10 mem-

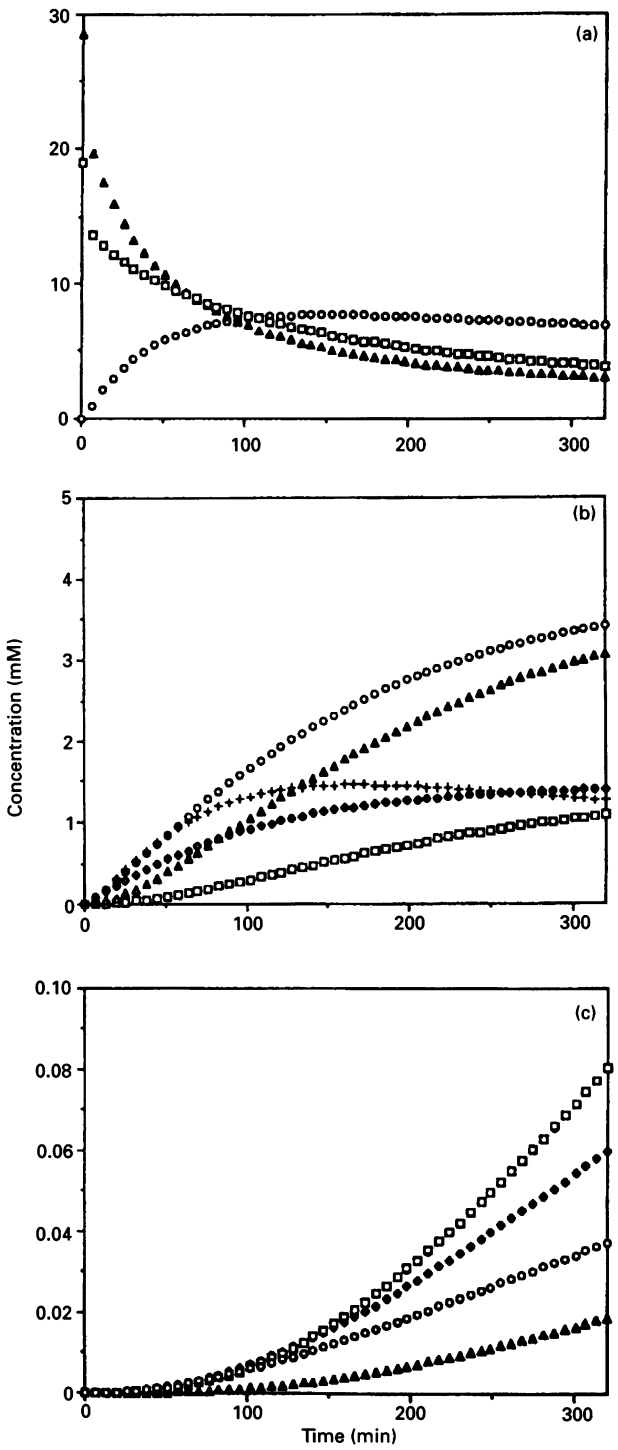

Figure 3 Computer simulation of the formation of isotopomers of Glc6*P* during the incubation of [U-^{13}C]Glc6*P*, Glc6*P* and Fru(1,6)P_2 with haemolysates

Simulations were carried out with the mathematical model of the non-oxidative pentose phosphate pathway described in Scheme 1; initial substrate concentrations were: [U-^{13}C]Glc6*P*, 28.5 mM; Glc6*P*, 19 mM; Fru(1,6,)P_2, 28.5 mM; DHAP, 5 μM; Fru6*P*, 5 μM; Glc(1,6)P_2, 50 μM; Rib5*P*, Sed(1,7)P_2 and Sed7*P* were set to 0.1 μM. The time axis was adjusted to correspond to an experiment carried out with haemolysates prepared from a 100%-haematocrit cell suspension; a correction to allow for the volume occupied by haemoglobin in the sample (Savitz et al., 1964) was also applied. The symbols denote the following: (**a**) ▲, [1,2,3,4,5,6-^{13}C]Glc6*P*; □, Glc6*P*; ○, [1,2,3-^{13}C]Glc6*P*; (**b**) ○, [1,2-^{13}C]Glc6*P*; ▲, [3-^{13}C]Glc6*P*; ◆, [3,4,5,6-^{13}C]Glc6*P*; +, [4,5,6-^{13}C]Glc6*P*; □, [1,2,4,5,6-^{13}C]Glc6*P*; (**c**) ◆, [1-^{13}C]Glc6*P* and [2-^{13}C]Glc6*P*; □, [2,3-^{13}C]Glc6*P* and [1,3-^{13}C]Glc6*P*; ○, [2,3,4,5,6-^{13}C]Glc6*P* and [1,3,4,5,6-^{13}C]Glc6*P*; ▲, [1,4,5,6-^{13}C]Glc6*P* and [2,4,5,6-^{13}C]Glc6*P*.

brane (molecular-mass cut-off 10000; Amicon, Danvers, MA, U.S.A.) using an Amicon ultrafiltration cell under 300 kPa of N_2 pressure. The filtrate was then freeze-dried and the powdered metabolites reconstituted in ^2H_2O, pH 7.4, for n.m.r. analysis.

N.m.r.

The ^{13}C DQF-COSY spectrum was acquired with a Bruker AMX-400 wb spectrometer at 100.62 MHz using a 10 mm-broadband probe tuned to the ^{13}C frequency. Broadband proton irradiation (WALTZ-16; Shaka et al., 1983) was applied continuously; the temperature was set to 298 K. The sample was contained in a 5 mm-diameter n.m.r. tube. The f_2 spectral width was 10000 Hz and was digitized into 4 k points; the f_1 spectral width was 10000 Hz with 512 increments with an acquisition time of 0.205 s; 160 transients were acquired for each increment. The intensities of cross-peaks were evaluated by manual integration using standard Bruker software (UXNMR, version 920501.6) following back-transformation of each selected row of the COSY to produce a free induction decay (f.i.d.) which was then transformed with greater digitization (32 k points).

N.m.r. time courses were acquired at 37 °C, which was the sample temperature achieved by setting the probe temperature below this value to compensate for the heating effect of broadband proton irradiation. The sample temperature was measured by acquiring a single-pulse ^{1}H spectrum of ethylene glycol contained in a capillary, immediately after switching off the broadband decoupling, according to the method of Bubb et al. (1988). The acquisitions of ^{13}C- and ^{31}P-n.m.r. spectra were interleaved, and the broadband ^{1}H decoupling (WALTZ-16) was applied continuously. The ^{13}C-n.m.r. acquisition parameters are given in the caption of Figure 1. Quantitative ^{31}P-n.m.r. time course spectra were acquired at a spectrometer frequency of 242.94 MHz and other experimental details are given in the caption of Figure 1. Assignments for ^{13}C-n.m.r. spectra were made by reference to previously reported chemical shifts (Arora et al., 1988); ^{31}P assignments were made by the addition of authentic compounds to an ultrafiltrate of the final sample and also by using chemical-shift-versus-pH data previously obtained in the authors' laboratory.

Computer simulations

Computer simulations were performed using the SCoP computer simulation package (National Biomedical Simulation Resource, Duke University Medical Center, Durham, NC, U.S.A.). The model incorporated the reactions of the classical non-oxidative pentose phosphate pathway as well as some additional reactions (Scheme 1) and was based on an earlier model developed in this laboratory (Kuchel et al., 1990). The relationships between the steady-state kinetic parameters and unitary rate constants were determined, following derivation of the rate equations for the enzyme reactions according to their published mechanisms (McIntyre et al., 1989). The model was modified by the iterative adjustment of the unitary rate constants, to achieve a closer visual match of the simulated metabolic flux profiles with ^{13}C- and ^{31}P-n.m.r. time-course data from incubations of various pentose-phosphate-pathway metabolites with haemolysates [Berthon et al. (1992) and time-course data presented here]. Additionally, the model was elaborated to include the equations for each isotopic entity [e.g. in principle there are 2^7 (128) possible ways a ^{13}C label may be distributed in sedoheptulose 7-phosphate (Sed7*P*), but only 32 ways according to Scheme 1];

the model contains a total of 434 isotopically distinct metabolites or enzyme complexes, with ten enzymes. (A copy of the SCoP input listing of the reactions and rate constants is available on request from P.W.K.; it has also been deposited as Supplementary Publication SUP 50174 (16 pages), which has been deposited at the British Library Document Supply Centre, Boston Spa, Wetherby, W. Yorkshire LS23 7BQ, from whom copies can be obtained on the terms indicated in Biochem. J. (1993) **289**, 9.) Simulated results were compared with experimental results by carrying out a time adjustment in which allowance was made for the haematocrit and the volume occupied by haemoglobin (Savitz et al., 1964) in experimental samples.

RESULTS

N.m.r. time-courses

The equilibria of the reactions comprising the non-oxidative pentose phosphate pathway lie heavily in favour of the formation of hexose phosphates, resulting in only slight changes in the composition of the sample (Figure 1). [1-^{13}C]Glc6*P* was rapidly isomerized to [1-^{13}C]Fru6*P*; the pentose phosphates ribulose 5-phosphate, xylulose 5-phosphate and ribose 5-phosphate (Ru5*P*, Xu5*P* and Rib5*P*) labelled at C-1 were also rapidly formed and remained present in the sample at a low concentration. The randomization of isotopic label due to the dynamic nature of the equilibria of the pathway was evident in the slow accumulation of isotopic labelling of Glc6*P* at C-3. [1,3-^{13}C]Glc6*P* arises from the formation of [1,3-^{13}C]Sed7*P* by the TK-mediated reaction of [1-^{13}C]Xu5*P* with [1-^{13}C]Rib5*P*, followed by the TA-catalysed transfer of the 'top' three-carbon unit of Sed7*P* on to glyceraldehyde 3-phosphate (G3*P*) to give [1,3-^{13}C]Fru6*P*, and subsequent isomerization to [1,3-^{13}C]Glc6*P*, viz.:

$$[1\text{-}^{13}\text{C}]\text{Xu5}P + \text{TK} \rightleftharpoons \text{TK–}[1\text{-}^{13}\text{C}]\text{Xu5}P$$

$$\text{TK–}[1\text{-}^{13}\text{C}]\text{Xu5}P \rightleftharpoons \text{TK–}[1\text{-}^{13}\text{C}]\text{glm} + \text{G3}P$$

$$\text{TK–}[1\text{-}^{13}\text{C}]\text{glm} + [1\text{-}^{13}\text{C}]\text{Rib5}P \rightleftharpoons \text{TK–}[1\text{-}^{13}\text{C}]\text{glm-}[1\text{-}^{13}\text{C}]\text{Rib5}P$$

$$\text{TK–}[1\text{-}^{13}\text{C}]\text{glm-}[1\text{-}^{13}\text{C}]\text{Rib5}P \rightleftharpoons \text{TK} + [1,3\text{-}^{13}\text{C}]\text{Sed7}P$$

$$[1,3\text{-}^{13}\text{C}]\text{Sed7}P + \text{TA} \rightleftharpoons \text{TA–}[1,3\text{-}^{13}\text{C}]\text{Sed7}P$$

$$\text{TA–}[1,3\text{-}^{13}\text{C}]\text{Sed7}P \rightleftharpoons \text{TA–}[1,3\text{-}^{13}\text{C}]\text{grn} + \text{Ery4}P$$

$$\text{TA–}[1,3\text{-}^{13}\text{C}]\text{grn} + \text{G3}P \rightleftharpoons \text{TA–}[1,3\text{-}^{13}\text{C}]\text{grn-G3}P$$

$$\text{TA–}[1,3\text{-}^{13}\text{C}]\text{grn-G3}P \rightleftharpoons \text{TA} + [1,3\text{-}^{13}\text{C}]\text{Fru6}P$$

$$[1,3\text{-}^{13}\text{C}]\text{Fru6}P \rightleftharpoons [1,3\text{-}^{13}\text{C}]\text{Glc6}P$$

where grn is the dihydroxyacetone moiety transferred by TA, glm is the glycolaldehyde moiety transferred by TK, and Ery4*P* is erythrose 4-phosphate.

The actions of phosphoglucomutase and phosphomannose isomerase were evident in the formation of [1-^{13}C]Glc1*P* and [1-^{13}C]Man6*P* respectively.

Fru(1,6)P_2 undergoes an aldolase-mediated reaction to yield G3*P* and dihydroxyacetone phosphate (DHAP). None of the reactions in Scheme 1 can result in the labelling of any of these three molecules, which are not observed in the ^{13}C-n.m.r. spectra, but may be followed in the ^{31}P-n.m.r. time course (Figure 1b). DHAP and Ery4*P* (also unlabelled by the reaction shown in Scheme 1) condense to form Sed(1,7)P_2, which was observed to accumulate slowly (Figure 1b).

Computer simulations

The metabolite concentration profiles determined experimentally, and by computer simulation, for the incubation of [1-^{13}C]Glc6*P*, Glc6*P* and Fru(1,6)P_2 with haemolysate are shown in Figure 2. As can be seen, the computer simulations match the experimental data well, displaying an initial sharp decrease in the concentration of [1-^{13}C]Glc6*P* due to isomerization to [1-^{13}C]Fru6*P*, followed by a gradual decline in concentration.

While the ^{13}C-n.m.r. time course with [1-^{13}C]Glc6*P* contains some information about the reactions which result in the

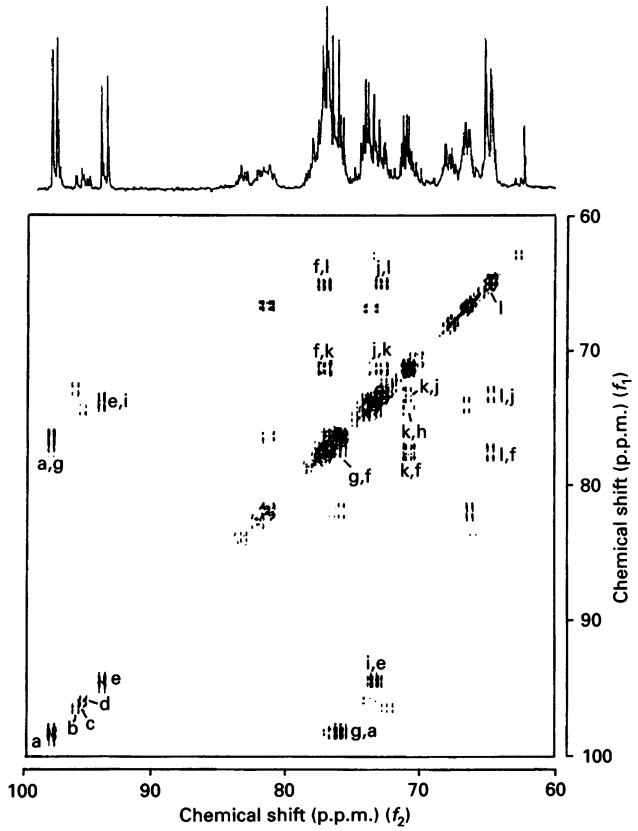

Figure 4 ^{13}C DQF-COSY of sample containing [U-^{13}C]Glc6*P* (28.5 mM), unsubstituted Glc6*P* (19 mM), and Fru(1,6)P_2 (28.5 mM) after incubation with haemolysate and subsequent deproteinization (see the Experimental section)

Acquisition parameters: spectrometer frequency, 100.62 MHz; acquisition time, 0.205 s; number of transients per increment, 160; 512 increments in f_1; 4 k data points in f_2; processing was with a phase-shifted sine function (shifted by $\pi/2$) applied in each dimension; f_1 was zero-filled to 1 k data points; broadband ^{1}H-decoupling (WALTZ-16) was applied continuously; set temperature, 298 K. Assignments: a, β Glc6*P* (C-1); b, β Man6*P* (C-1); c, α Man6*P* (C-1); d, Glc1*P* (C-1); e, α Glc6*P* (C-1); f, β Glc6*P* (C-3, C-5); g, β Glc6*P* (C-2); h, α Glc6*P* (C-3); i, α Glc6*P* (C-2); j, α Glc6*P* (C-5); k, α,β Glc6*P* (C-4); l, α,β Glc6 *P* (C-6) (not all letters are shown on the diagonal of the spectrum); the cross-peaks are labelled with the f_2 assignment followed by the f_1 assignment; the following assignments of cross-peaks are explicitly given as there is some ambiguity due to co-resonance of peaks: f,k, β Glc6*P* (C-3, C-5), β Glc6*P* (C-4); f,l, β Glc6*P* (C-5), β Glc6*P* (C-6); g,f, β Glc6*P* (C-2), β Glc6*P* (C-3); j,k, α Glc6*P* (C-5), α Glc6*P* (C-4); j,l, α Glc6*P* (C-5), α Glc6*P* (C-6); k,f, β Glc6*P* (C-4), β Glc6*P* (C-3, C-5); k,h, α Glc6*P* (C-4), α Glc6*P* (C-3); k,j, α Glc6*P* (C-4), α Glc6*P* (C-5); l,f, β Glc6*P* (C-6), β Glc6*P* (C-5); l,j, α Glc6*P* (C-6), α Glc6*P* (C-5).

Figure 5 Cross-peaks from selected rows of the DQF-COSY spectrum (Figure 4)

For acquisition parameters, see Figure 4; for processing parameters, see the Experimental section. Assignments: (**a**) (a,g) β Glc6*P* $C_{12}{}^{1}$; (**b**) (g,a) β Glc6*P* $C_{12}{}^{2}$, the '*a*' and '*b*' on this peak refer to the AMX (doublet of doublets) and AM (doublet) coupled spins respectively; (**c**) (i,e) α Glc6*P* $C_{12}{}^{2}$; (**d**) (g,f) βGlc6*P* $C_{23}{}^{2}$; (**e**) (k,h) α Glc6*P* $C_{34}{}^{4}$; (**f**) (k,j) α Glc6*P* $C_{45}{}^{4}$; (**g**) (j,k) α Glc6*P* $C_{45}{}^{5}$; (**h**) (f,l) β Glc6*P* $C_{56}{}^{5}$; (**i**) (l,f) β Glc6*P* $C_{56}{}^{6}$.

catabolism and re-formation of hexose phosphate molecules (e.g. the accumulation of isotopic label at C-3 of Glc6*P*), this information is incomplete, as many of the bidirectional reactions will result in the re-formation of hexose phosphate molecules which have a labelling pattern identical with that present originally. For example, the operation of the TA reaction, which utilizes [1-^{13}C]Fru6*P* and Ery4*P* as substrates, converting them into G3*P* and [1-^{13}C]Sed7*P*, and then back to [1-^{13}C]Fru6*P* and Ery4*P* again, will not be identified by ^{13}C n.m.r. However, with [U-^{13}C]Glc6*P* and Glc6*P* as initial substrates, a wide array of isotopomers may potentially be formed, thus creating the opportunity to detect exchange reactions. The mathematical model of the non-oxidative pentose phosphate pathway was therefore used to simulate an experiment in which [1-^{13}C]Glc6*P* was replaced with [U-^{13}C]Glc6*P*.

The computer simulations predicted that the transaldolase 'exchange' reaction should dominate the randomization of isotopic label, with [1,2,3-^{13}C]Glc6*P* rapidly rising in concentration (Figure 3a) at an initial rate of 122 μmol·min^{-1}·l^{-1} (calculated by the fitting of a phenomenological polynomial of degree 3 to the initial four points in the 50-step computer simulation). This 'exchange' is due to the reactions:

[1,2,3,4,5,6-^{13}C]Fru6*P* + TA $\rightleftharpoons$ TA–[1,2,3-^{13}C]grn-[1,2,3-^{13}C]G3*P*

TA–[1,2,3-^{13}C]grn-[1,2,3-^{13}C]G3*P* $\rightleftharpoons$ TA–[1,2,3-^{13}C]grn + [1,2,3-^{13}C]G3*P*

G3*P* + TA–[1,2,3-^{13}C]grn $\rightleftharpoons$ TA–[1,2,3-^{13}C]grn-G3*P*

TA–[1,2,3-^{13}C]grn-G3*P* $\rightleftharpoons$ TA + [1,2,3-^{13}C]Fru6*P*

Overall

[1,2,3,4,5,6-^{13}C]Fru6*P* + G3*P* $\rightleftharpoons$ [1,2,3-^{13}C]Fru6*P* + [1,2,3-^{13}C]G3*P*

The concentration of [1,2-^{13}C]Glc6*P* increased at an initial rate of 8.9 μmol·min^{-1}·l^{-1} (Figure 3b). The scission of C-2–C-3 bonds reflected the activity of transketolase, viz.:

Fru6*P* + TK $\rightleftharpoons$ TK–glm – Ery4*P*

TK–glm – Ery4*P* $\rightleftharpoons$ TK–glm + Ery4*P*

[1,2,3,4,5,6-^{13}C]Fru6*P* + TK $\rightleftharpoons$ TK–[1,2-^{13}C]glm – [1,2,3,4-^{13}C]Ery4*P*

TK–[1,2-^{13}C]glm-[1,2,3,4-^{13}C]Ery4*P* $\rightleftharpoons$ TK–[1,2-^{13}C]glm + [1,2,3,4-^{13}C]Ery4*P*

Ery4*P* + TK–[1,2-^{13}C]glm $\rightleftharpoons$ TK–[1,2-^{13}C]glm – Ery4*P*

TK–[1,2-^{13}C]glm – Ery4*P* $\rightleftharpoons$ TK + [1,2-^{13}C]Fru6*P*

Overall

Fru6*P* + [1,2,3,4,5,6-^{13}C]Fru6*P* + TK $\rightleftharpoons$ TK–glm + [1,2,3,4-^{13}C]Ery4*P* + [1,2-^{13}C]Fru6*P*

[4,5,6-^{13}C]Glc6*P* was formed at an initial rate of 6.8 μmol·min^{-1}·l^{-1}, and [3,4,5,6-^{13}C]Glc6*P*, [3-^{13}C]Glc6*P* and [1,2,4,5,6-^{13}C]Glc6*P* were produced at 8.7 μmol·min^{-1}·l^{-1},

Table 1 Comparison of isotopomer ratios of Glc6*P* derived from computer simulations and the DQF-COSY spectrum

Notes: [a]the theoretical isotopomer ratios were obtained by computer simulation with the mathematical model described in Scheme 1 and the initial conditions as described in Figure 3. [b]The ratios were determined with the equation: ratio = $2a/(2a+b)$, where a is the intensity of the outer peak of each AM multiplet showing coupling to X and b is the intensity of the central peak with no additional coupling to X (see Figure 5b); a is multiplied by 2 to account for its coupled peak which was usually obscured in the centre of the multiplet. The ratio quoted is the average of determinations from each side of the centroid of the multiplet. The experimentally determined ratios were obtained from: [c]βGlc6*P* $C_{12}{}^2$ cross-peak; [d]βGlc6*P* $C_{23}{}^2$ cross-peak; [e]the βGlc6*P* $C_{23}{}^3$ cross-peak, although there is more uncertainty in this value due to the poor resolution obtained for this cross-peak; [f]αGlc6*P* $C_{34}{}^3$ cross-peak, although there is also considerable uncertainty in this value due to the poor signal-to-noise ratio obtainable for this cross-peak; [g]αGlc6*P* $C_{34}{}^4$ cross-peak; [h]αGlc6*P* $C_{45}{}^4$ cross-peak; [i]αGlc6*P* $C_{45}{}^5$ cross-peak and [j]βGlc6*P* $C_{56}{}^5$ cross-peak.

	Cxyz/Cyz ratio (%)	
Cxyz/Cyz	Theoretical[a]	Experimentally determined[b]
C123/C12	69	82[c]
C123/C23	99	100[d]
C234/C23	31	20–40[e]
C234/C34	68	80[f]
C345/C34	100	100[g]
C345/C45	66	62[h]
C456/C45	100	100[i]
C456/C56	100	100[j]

0.27 μmol·min^{-1}·l^{-1}, and 0.007 μmol·min^{-1}·l^{-1} respectively (Figure 3b). All other isotopomers formed were of minor concentration (Figure 3c).

COSY spectrum

The array of isotopomers resulting from the incubation for 10 h of [U-^{13}C]Glc6*P*, Glc6*P* and Fru(1,6)P_2 with a haemolysate was detected by examining the cross-peaks of the ^{13}C-DQF-COSY spectrum. The βGlc6*P* $C_{12}{}^1$ cross-peak (Figure 5a) from the COSY spectrum (Figure 4) exhibits a simple coupling pattern resulting from active coupling between carbons 1 and 2 (C-1 and C-2). As might be expected, there is no evidence of additional coupling of C-1 to any other carbon nucleus. The coupling pattern from the cross-peak of βGlc6*P* $C_{12}{}^2$ (Figure 5b) is more complex: a proportion of C-2 nuclei coupled to C-1 nuclei are also coupled to C-3 nuclei; this is reflected in the presence of both active coupling (from coupling between C-1 and C-2) and passive coupling (from C-2 and C-3). Because the magnitudes of these coupling constants are similar, some cancellation of signal is observed in the centre of the multiplet. The peaks in the middle of the positive and negative portions of the multiplet (denoted *b*) result from the C-2 nuclei which are coupled to C-1 nuclei only; in this case no resultant passive coupling is observed, and this signal is superimposed upon the pattern derived from fully coupled C123 groups. The multiplet pattern observed with the β-anomer is also apparent in the α-anomeric form (Figure 5c). The C23 cross-peaks are poorly resolved in the COSY spectrum, owing to the proximity in the chemical shifts of the resonances from C-2 and C-3 of both the α- and β-anomers of Glc6*P* (Arora et al., 1988). From the cross-peak of βGlc6*P* $C_{23}{}^2$ (Figure 5d), it may be observed that approximately all intact C23 units are also coupled to C-1. Additionally, an estimate of the proportion of C23 units also attached to C-4 may be derived from the βGlc6*P*$_{23}{}^3$ peak, which shows responses from combined active and passive coupling as well as from active coupling only. The signal-to-noise ratio of the C34 cross-peaks is considerably poorer than for the C12 cross-peaks, indicating that fewer C34 units remain intact. The chemical shifts of C-3 and C-5 of βGlc6*P* are very close (within 0.1 p.p.m.), and the cross-peaks are superimposed. The αGlc6*P* $C_{34}{}^3$ cross-peak exhibits a coupling pattern which is consistent with not all the C34 groups being correlated to C-2 nuclei. In the αGlc6*P* $C_{34}{}^4$ cross-peak, most C34 units are also correlated to C-5 nuclei (Figure 5e). The αGlc6*P* $C_{45}{}^4$ peak (Figure 5f) is composed of the responses of C345 and C45 units superimposed upon each other, providing further evidence that a proportion of C34 links are broken. The αGlc6*P* $C_{45}{}^5$ (Figure 5g) and the βGlc6*P* $C_{56}{}^5$ (Figure 5h) exhibit patterns consistent with all C456 units of Glc6*P* remaining intact. A comparison of the experimentally obtained isotopomer ratios and the results from computer simulations is given in Table 1.

DISCUSSION

The ^{13}C-DQF-COSY experiment offers a novel and easily applied method for detecting exchange reactions which result in the transfer of groups of carbon atoms from one molecule to another. While radioactive label distributions have been used to characterize these reactions, the extent of such reactions has largely defied quantification. Thus the ^{13}C-COSY technique represents an especially useful approach with the potential for measuring chemical flux and isotopic exchange independently. ^{13}C COSY was particularly well-suited to the study of the 'reverse' operation of the non-oxidative pentose phosphate pathway, because the equilibria of the enzymic reactions favour hexose phosphate formation, so the final mixture for analysis was not complicated by large amounts of other labelled metabolites.

The resonances marked '*b*' in the $C_{12}{}^2$ cross-peak of both α- and β-Glc6*P* (Figure 5b) in the COSY spectrum lie slightly to higher frequency of the doublets arising from additional coupling of C-2 to C-3. This high-order effect (London, 1988) is quite small, and the potential error in the quantification of isotopomer proportions may be obviated by taking an average of ratios from each side of the centroid of the multiplet under analysis (Table 1). For protonated ^{13}C nuclei, the relaxation effects arising from ^{13}C–^{13}C interactions are small and may be safely neglected in the analysis, owing to the domination of the ^{13}C–^{1}H dipolar interaction (London, 1988). Thus the relative intensities of resonances within cross-peaks would not be significantly affected by differing rates of relaxation. Processing of the COSY was with a sine function, phase-shifted by $\pi/2$, to minimize potential errors in the evaluation of the integrals of cross-peak multiplets associated with distorting the initial portion of the f.i.d. (Neuhaus and Williamson, 1989).

The use of the ^{13}C isotope offers several advantages over the more widely employed ^{14}C isotope. As well as being non-destructive to the sample, more than one ^{13}C nucleus may be simultaneously and directly detected with n.m.r. spectroscopy. Furthermore, the presence and relative proportions of different ^{13}C isotopomers of the same metabolite can be evaluated by the analysis of ^{13}C–^{13}C homonuclear spin-coupling patterns [London et al., 1975; Walker et al., 1982; Sherry et al., 1985; Kalderon et al., 1986; Malloy et al., 1987, 1990; London, 1988 (and references cited therein); Cerdan and Seelig, 1990; Jeffrey et al., 1991]. The diagnosis and classification of some enzymopathies in humans by ^{13}C-isotopomer analysis has been described by Lapidot and co-workers (Kalderon et al., 1989; Gopher et al., 1990). The

metabolic features of the diseases studied were indicated by the coupling patterns, which reflected the presence of different metabolite isotopomers in ^{13}C n.m.r. spectra of plasma samples. Our study has used two-dimensional spectroscopy to obtain adequate resolution to observe the multiplet structure of resonances within the crowded ^{13}C-n.m.r. spectrum.

The mathematical model employed to simulate the experimental results incorporated each possible isotopic form of all of the pathway metabolites, as well as the rate constants describing the formation of each enzyme–substrate complex of the modified classical pentose phosphate pathway (Scheme 1). Thus the quantification, by computer simulation, of the role of 'exchange' reactions was an automatic consequence of the ability of our model to describe the metabolic pathway (Berthon et al., 1992). This approach represents a considerable improvement over the qualitative invocation of particular isotopic exchange reactions in order to explain data from ^{14}C-labelling experiments (e.g. Williams et al., 1978, 1987; Longenecker and Williams, 1980a,b; Williams and Blackmore, 1983). Katz and Rognstad (1967) have constructed a 'phenomenological' mathematical model describing the incorporation of isotopic label into various intermediates of the non-oxidative pentose phosphate pathway in terms of flux rates. They used the labelling distributions observed experimentally following the incubation of *Escherichia coli*, regenerating rat liver *in vivo*, and rat muscle and Hela cells *in vivo*, with radioactively labelled substrates to obtain sets of flux rates which were incorporated into the computer model. In contrast, our model is constructed from equations which reflect the underlying kinetic mechanism of each enzymic reaction, with adjustments in order to achieve a greater degree of matching between simulated metabolite concentration profiles and those derived from n.m.r.-time-course experiments. For most enzymes, reasonable agreement between the published values for the steady-state parameters and those derived from the unitary rate constants incorporated in the model has been achievable (McIntyre et al., 1989; Berthon et al., 1992). The results obtained in this work corroborate the findings of Crawford and Blum (1983), who noted high rates of bidirectional carbon flow in their numerical investigations of the pentose phosphate pathway in isolated rat hepatocytes. While the net chemical flux occurring during the incubation was small, owing to the equilibria of the reactions of the non-oxidative pentose phosphate pathway lying in favour of the formation of hexose phosphates, evidence for considerable exchange of isotopic label in Glc6*P* was obtained.

The initial sample composition was chosen to provide optimal conditions for the reversal of flux through the non-oxidative pentose phosphate pathway (in the direction of pentose phosphate formation). To facilitate isotopic redistribution, the experimental sample contained Fru(1,6)P_2, which serves as a source of G3*P* (Scheme 1), as well as Glc6*P*. Under these conditions, the degree of isotopic redistribution would be expected to be large, owing to the low amount of net flux. This approach was also used by Williams and Blackmore (1983) in their investigation of the operation of the pentose phosphate pathway in a rat liver enzyme extract.

In contrast with Williams and Blackmore (1983), who found no evidence for the involvement of the TA reactions in the pentose phosphate pathway in a rat liver extract, our results, with human erythrocytes, are well described by a scheme of reactions which includes the TA-catalysed transfer of a three-carbon unit between Sed7*P* and Fru6*P*. A low intensity cross-peak between C-3 and C-4 of Glc6*P* was detected in the COSY spectrum (Table 1), reflecting the influence of TA in the scission of the C-3–C-4 bond of Fru6*P*. Simulations of the isotopomers formed when the transaldolase activity was set to zero (Figure 6),

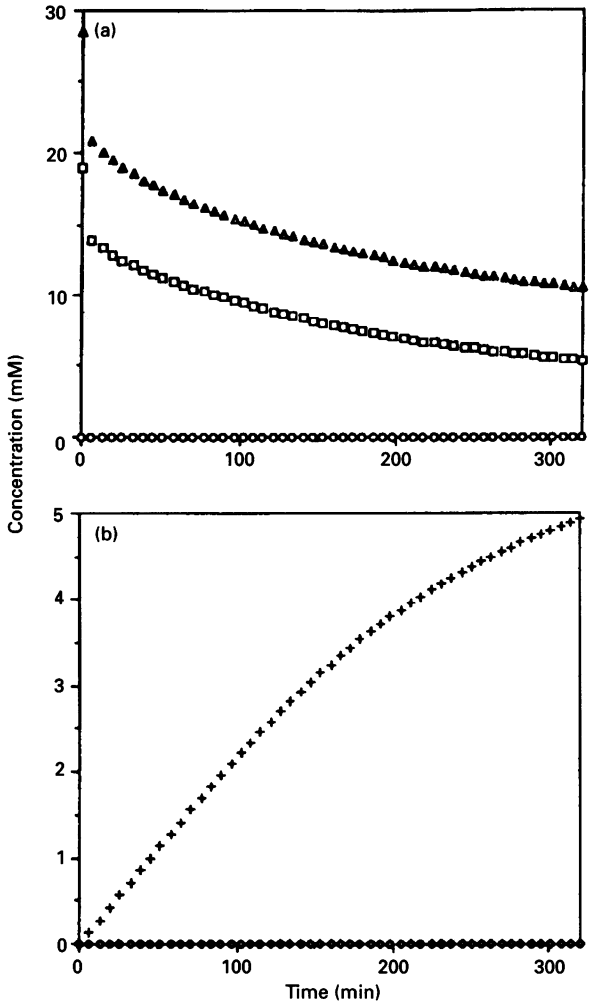

Figure 6 Computer simulation of the formation of isotopomers of Glc6*P* during the incubation of [U-^{13}C]Glc6*P*, Glc6*P* and Fru(1,6,)P_2 with haemolysates in the absence of transaldolase

Simulations were carried out with the mathematical model of the non-oxidative pentose phosphate pathway given in Scheme 1; all enzyme and substrate concentrations were the same as those given in Figure 3, except that the concentration of TA was set to zero. The symbols denote the following: (**a**) △, [1,2,3,4,5,6-^{13}C]Glc6*P*; □, Glc6*P*; ○, [1,2,3-^{13}C]Glc6*P*; (**b**) +, [3,4,5,6-^{13}C]Glc6*P* and [1,2-^{13}C]Glc6*P*; ◇, [3-^{13}C]Glc6*P*, [4,5,6-^{13}C]Glc6*P* and [1,2,4,5,6-^{13}C]Glc6*P*.

showed that isotopomers such as [1,2,3-^{13}C]Glc6*P*, [4,5,6-^{13}C]Glc6*P* and [1,2,4,5,6-^{13}C]Glc6*P*, were not formed at all, and the isotopomers expected to be formed by the action of TK, namely [1,2-^{13}C]Glc6*P* and [3,4,5,6-^{13}C]Glc6*P*, had a greater preponderance. Thus the results presented in this work can be adequately described by the classical scheme of reactions for the non-oxidative pentose phosphate pathway.

Finally, the ^{13}C-COSY technique enabled the investigation of bidirectional enzymic reactions and offers the potential for further study of the reactions occurring within the human red blood cell. The acquisition of time courses of ^{13}C COSY spectra would provide useful data for the further characterization of the kinetics of these exchange reactions by allowing the time-dependent formation of isotopomers of Glc6*P* to be monitored. In the present work, the labelled substrate, [1-^{13}C]Glc6*P*, was used instead of [U-^{13}C]Glc6*P* to monitor the time course of changes in metabolite levels with ^{13}C n.m.r. The computer model showed

satisfactory agreement with both the time-course data (obtained using [1-^{13}C]Glc6*P*) and the isotopomer ratios determined from the COSY spectrum of the final sample (obtained using [U-^{13}C]Glc6*P*) following the 10 h incubation with a haemolysate.

Conclusions

We have demonstrated the utility of ^{13}C-COSY spectra for studying exchange reactions under conditions of minimal net pathway flux in human haemolysates. Although the equilibria of the non-oxidative pentose phosphate pathway in human erythrocytes favour the formation of hexose phosphates, the operation of exchange reactions involving hexose phosphate molecules was demonstrated to be extensive. An analysis of the isotopic forms of Glc6*P*, manifested in the multiplet patterns of cross-peaks in the ^{13}C-COSY spectrum of the incubation sample, was consistent with predictions based on a computer model which incorporated the reactions of the 'classical' scheme of the non-oxidative pentose phosphate pathway, with TA playing an important role in bringing about the label redistribution that was observed.

This work was supported by a grant to P.W.K. from the Australian National Health and Medical Research Council. H.A.B. received an Australian Postgraduate Research Award from the Commonwealth Government and support from the Cooperative Research Centre for Molecular Engineering and Technology: Sensing and Diagnostic Technologies. Dr. J. Mailen Kootsey (National Biomedical Simulation Resource, Duke University Medical Center, Durham, NC, U.S.A.; N.I.H. grant RR01693) is thanked for the supply of the computer program SCoP. Mr. Bill Lowe and Mr. Brian Bulliman are thanked for their technical and computing assistance respectively. The advice of Dr. U. Peter Lundberg, with respect to the processing of the COSY spectrum, is gratefully acknowledged.

REFERENCES

Arora. K. K., Longenecker, J. P. and Williams, J. F. (1987) Int. J. Biochem. **19**, 133–146
Arora, K. K., Collins, J. G., MacLeod, J. K. and Williams, J. F. (1988) Biol. Chem. Hoppe-Seyler **369**, 549–557
Bartlett, G. R. (1968) Biochim. Biophys. Acta **156**, 221–230
Bartlett, M. R. E., Collins, J. G., Flanigan, I., MacLeod, J. K. and Williams, J. F. (1989) Biochem. Int. **18**, 35–46
Berthon, H. A., Kuchel, P. W. and Nixon, P. F. (1992) Biochemistry **31**, 12792–12798
Bubb, W. A., Kirk, K. and Kuchel, P. W. (1988) J. Magn. Reson. **77**, 363–368
Butler, R. N., Arora, K. K., Collins, J. G., Flanigan, I., Lawson, M. J., Roberts-Thomson, I. C. and Williams, J. F. (1990) Biochem. Int. **22**, 249–260
Cerdan, S. and Seelig, J. (1990) Annu. Rev. Biophys. Biophys. Chem. **19**, 43–67

Received 18 February 1993/15 June 1993; accepted 8 July 1993

Clark, M. G., Williams, J. F. and Blackmore, P. F. (1971) Biochem. J. **125**, 381–384
Cohen, S. M., Rognstad, R., Shulman, R. G. and Katz, J. (1981) J. Biol. Chem. **256**, 3428–3432
Crawford, J. M. and Blum, J. J. (1983) Biochem. J. **212**, 595–598
Gopher, A., Vaisman, N., Mandel, H. and Lapidot, A. (1990) Proc. Natl. Acad. Sci. U.S.A. **87**, 5449–5453
Graham, D. and Smydzuk, J. (1965) Anal. Biochem. **11**, 246–255
Jeffrey, F. M. H., Rajagopal, A., Malloy, C. R. and Sherry, A. D. (1991) Trends Biochem. Sci. **16**, 5–10
Jones, D. N. M. and Sanders, J. K. M. (1989) J. Am. Chem. Soc. **111**, 5132–5137
Kalderon, B., Gopher, A. and Lapidot, A. (1986) FEBS Lett. **204**, 29–32
Kalderon, B., Korman, S. H., Gutman, A. and Lapidot, A. (1989) Proc. Natl. Acad. Sci. U.S.A. **86**, 4690–4694
Katz, J. and Rognstad, R. (1967) Biochemistry **6**, 2227–2247
Kuchel, P. W. and Chapman, B. E. (1985) Experientia **41**, 53–55
Kuchel, P. W., Berthon, H. A., Bubb, W. A., Bulliman, B. T. and Collins, J. G. (1990) Biomed. Biochim. Acta **49**, 757–770
Landau, B. R. and Bartsch, G. E. (1966) J. Biol. Chem. **241**, 741–749
Landau, B. R. and Wood, H. G. (1983) Trends Biochem. Sci. **8**, 292–296
Ljungdahl, L., Wood, H. G., Racker, E. and Couri, D. (1961) J. Biol. Chem. **236**, 1622–1625
London, R. E. (1988) Prog. NMR Spectrosc. **20**, 337–383
London, R. E., Kollman, V. H. and Matwiyoff, N. A. (1975) J. Am. Chem. Soc. **97**, 3565–3573
Longenecker, J. P. and Wiliams, J. F. (1980a) Biochem. J. **188**, 859–865
Longenecker, J. P. and Wiliams, J. F. (1980b) Biochem. J. **188**, 847–857
Malloy, C. R., Sherry, A. D. and Jeffrey, F. M. H. (1987) FEBS Lett. **212**, 58–62
Malloy, C. R., Sherry, A. D. and Jeffrey, F. M. H. (1990) Am. J. Physiol. **259**, H987–H995
McIntyre, L. M., Thorburn, D. R., Bubb, W. A. and Kuchel, P. W. (1989) Eur. J. Biochem. **180**, 399–420
Neuhaus, D. and Williamson, M. (1989) in The Nuclear Overhauser Effect In Structural and Conformational Analysis, pp. 294–296, VCH Publishers, New York
Paoletti, F., Williams, J. F. and Horecker, B. L. (1979) Arch. Biochem. Biophys. **198**, 614–619
Savitz, D., Sidel, V. W. and Solomon, A. K. (1964) J. Gen. Physiol. **48**, 79–94
Scofield, R. F., Kosugi, K., Chandramouli, V., Kumaran, K., Schumann, W. C. and Landau, B. R. (1985) J. Biol. Chem. **260**, 15439–15444
Scott, A. I. and Baxter, R. L. (1981) Annu. Rev. Biophys. Bioeng. **10**, 151–174
Shaka, A. J., Keeler, J. and Freeman, R. (1983) J. Magn. Reson. **53**, 313–340
Sherry, A. D., Nunnally, R. L. and Peshock, R. M. (1985) J. Biol. Chem. **260**, 9272–9279
Walker, T. E., Han, C. H., Kollman, V. H., London, R. E. and Matwiyoff, N. A. (1982) J. Biol. Chem. **257**, 1189–1195
Williams, J. F. (1980) Trends Biochem. Sci. **5**, 315–320
Williams, J. F. and Blackmore, P. F. (1983) Int. J. Biochem. **15**, 797–816
Williams, J. F., Rienits, K. G., Schofield, P. J. and Clark, M. G. (1971) Biochem. J. **123**, 923–943
Williams, J. F., Blackmore, P. F. and Clark, M. G. (1978) Biochem. J. **176**, 257–282
Williams, J. F., Gordon, R. D., Gerdes, R. G., Rienits, K. G., Arora, K. K. and Anderson, J. (1986) Biochem. Int. **13**, 321–333
Williams, J. F., Arora, K. K. and Longenecker, J. P. (1987) Int. J. Biochem. **19**, 749–817